Reactions $K^-p \to \Sigma^\pm\pi^\mp$ at 4.07 and 5.47 GeV/c*

J. S. Loos,† U. E. Kruse, and E. L. Goldwasser‡
Department of Physics, University of Illinois, Urbana, Illinois
(Received 29 March 1968)

Experimental results, based on a hydrogen-bubble-chamber exposure, are reported for the reactions (1) $K^-p \to \Sigma^+\pi^-$ and (2) $K^-p \to \Sigma^-\pi^+$. In the experiment, K^- track lengths equivalent to 0.95 μb per event at 4.07 GeV/c and 0.27 μb per event at 5.47 GeV/c have been analyzed. The cross sections at 4.07 and 5.47 GeV/c, respectively, are 107 ± 27 and 84 ± 14 μb for reaction (1), and 8 ± 5 and 2 ± 1 μb for reaction (2). The dominant feature of reaction (1) is a peripheral peak in the center-of-mass production angular distribution. Differential cross sections are presented for the pheripheral region, and a comparison with the Regge model of Sarma and Reeder is made. Because of the statistics of this experiment, only crude estimates can be given for the extreme backward (antiperipheral) differential cross section for these reactions.

I. INTRODUCTION

We report on the following reactions from K^-p interactions at 4.07 and 5.47 GeV/c:

$$K^-p \to \Sigma^+\pi^-, \quad (1)$$

$$K^-p \to \Sigma^-\pi^+. \quad (2)$$

Above 2 GeV/c, experiments on reactions (1) and (2) have been reported at 2.24,[1] 3.0,[2] and 3.5 GeV/c.[3] In this energy region the two reactions have quite different characteristics, although both exhibit familiar properties of two-body and quasi-two-body reactions.[4,5] In terms of a one-particle-exchange picture, reaction (1) can proceed either by meson exchange or by baryon exchange, whereas reaction (2) can proceed only by baryon exchange. Existing data on these reactions seem to confirm such exchanges.

Reaction (1) has been interpreted in terms of the Regge-pole model by Iwao,[6] by Arnold,[7] and recently by Sarma and Reeder.[8] In the phenomenological analysis of Sarma and Reeder, a search is made for a set of parameters which can account for a wide range of experimental data on hypercharge-exchange reactions. Our experimental data on reaction (1) are part of the input data used by Sarma and Reeder to find such a set of parameters, and we find that their parametrization provides a reasonable fit to our data.

In Sec. II, a brief account of the data reduction and analysis procedures is given. Our experimental results on reactions (1) and (2) are presented in Sec. III and compared with other experiments in Sec. IV. In Sec. V, we discuss reaction (1) in terms of the Regge-pole model, with particular emphasis on the analysis of Sarma and Reeder.

II. DATA REDUCTION AND ANALYSIS PROCEDURES

The data were obtained using the Argonne separated-beam-transport system[9] and the MURA 30-in. bubble chamber.[10] K^- track lengths equivalent to 0.95 μb per event at 4.07 GeV/c and 0.27 μb per event at 5.47 GeV/c have been analyzed. The K^- track lengths in the exposure were determined by a beam-track-count method and checked with a count of K^- τ decays.

Reactions (1) and (2) appear in the bubble chamber as two-prong events with a charged decay, or "kink," on the hyperon track. Two independent scans were made of the film in a search for events with a visible "kink." Certain geometric or kinematic configurations can, of course, make the "kink" signature difficult to see at the scanning table. In particular, we expect a systematic loss of events for which either (a) the Σ track is very short or (b) the laboratory decay angle between the Σ track and its charged decay product (kink angle) is very small. The first systematic loss is associated primarily with events having a low-momentum Σ particle; the second is associated primarily with events having a high-momentum Σ particle. In the Appendix, we provide a detailed account of how we have handled the problem of systematic detection losses; our basic approach to the problem is briefly outlined here. First, the following acceptance criteria are applied to each observed event: (a) The Σ track length must exceed 0.5 cm, and (b) the laboratory angle between the Σ and its charged decay product must exceed 7°. Then, for each accepted event we compute a weight that is the

* Work supported in part by the U. S. Atomic Energy Commission.
† Based on a thesis submitted in partial fulfillment of the requirements for the Ph.D. degree at the University of Illinois, Urbana, Ill.
‡ Present address: National Accelerator Laboratory, Oak Brook, Ill.
[1] G. W. London, R. R. Rau, N. P. Samios, S. S. Yamamoto, M. Goldberg, S. Lichtman, M. Primer, and J. Leitner, Phys. Rev. 143, 1034 (1966).
[2] Paris-Saclay-Amsterdam Collaboration, Centre d'Etude Nucléaire, Saclay, Report No. CEA-R3037, 1966 (unpublished).
[3] Birmingham-Glasgow-London (I.C.)-Oxford-Rutherford Collaboration, Phys. Rev. 152, 1148 (1966).
[4] J. D. Jackson, Rev. Mod. Phys. 37, 484 (1965).
[5] J. D. Jackson, in *Proceedings of the Thirteenth International Conference on High-Energy Physics, Berkeley, 1966* (University of California Press, Berkeley, 1967), p. 149.
[6] S. Iwao, Nuovo Cimento 28, 1246 (1963).
[7] R. C. Arnold, Phys. Rev. 153, 1506 (1967).
[8] K. Sarma and D. Reeder, Nuovo Cimento 53, 808 (1968); D. Reeder and K. Sarma, Phys. Rev. (to be published).
[9] T. H. Fields, E. L. Goldwasser, and U. E. Kruse, Argonne National Laboratory Report No. THF/ELG/UEK-1, 1961 (unpublished).
[10] J. A. Froelich, Argonne National Laboratory Report No JAF-1, 1965 (unpublished).

TABLE I. Cross sections for $K^-p \to \Sigma^\pm\pi^\mp$.

K^- momentum (GeV/c)	$\sigma(\Sigma^+\pi^-)$ (μb)	$\sigma(\Sigma^-\pi^+)$ (μb)
4.07	107±27	8±5
5.47	84±14	2±1

product of two factors. The first factor is simply the reciprocal of the probability that the event satisfies the imposed cutoffs; the second is an empirically determined factor which provides additional weighting to events that occur near the cutoff limits where the detection efficiency is falling off.

In addition to the strong systematic scanning losses near the cutoffs, there are smaller "random" scanning losses probably due to chance oversight by the scanner and assumed to be independent of the systematic losses. In order to evaluate the random scanning losses, we have investigated a sample of 70 identified events from reactions (1) and (2) for which the Σ has a length greater than 1.2 cm and for which the Σ laboratory decay angle exceeds 10°. These events are far enough away from the cutoffs so that the strong systematic Σ detection losses are expected to be small. By comparing the results of the two independent scans, it is found that the overall random scanning loss for reactions (1) and (2) is 4%.

The candidates found in scanning were measured on a conventional film-plane measuring machine having a screw-driven stage with a least count of 1 μ. The precision of this machine was found to be adequate for the digitization of the difficult Σ events. In all, about 1000 candidates for reactions (1) and (2) were measured in the 4.07-GeV/c data and about 2200 were measured in the 5.47-GeV/c data.

Spatial reconstruction and kinematic fitting of the measured events were carried out by the SPACE-EUCLID-ILLFIT system developed at the University of Illinois. The kinematic fitting is done in two steps. First, the decay vertex is fitted for energy and momentum balance: $\Sigma^+ \to \pi^+ n$, $\Sigma^+ \to p\pi^0$, or $\Sigma^- \to \pi^- n$.[11] Second, the production vertex is fitted for various hypotheses (e.g., $\Sigma\pi$, $\Sigma\pi\pi$, or $\Sigma K\bar{K}$), using the results of the preceding fit to provide the Σ momentum. The $\Sigma\pi$ hypotheses have four kinematic constraints and are easily separated from competing hypotheses simply on the basis of kinematic fitting. The only ambiguity in interpretation which remained after kinematic fitting concerned the choice between decay modes for reaction (1). This ambiguity occurred for about 2% of the identified events and could be resolved in every case by track-density estimates. As a check on our analysis procedure, we have

[11] These decay hypotheses have one kinematic constraint when the directions and curvatures of the incoming Σ and outgoing charged decay product are known. Often, however, the curvature of the Σ track is not known or is very poorly known, so that there are no kinematic constraints; in such cases, there are two solutions or "roots" which provide energy and momentum balance at the decay vertex.

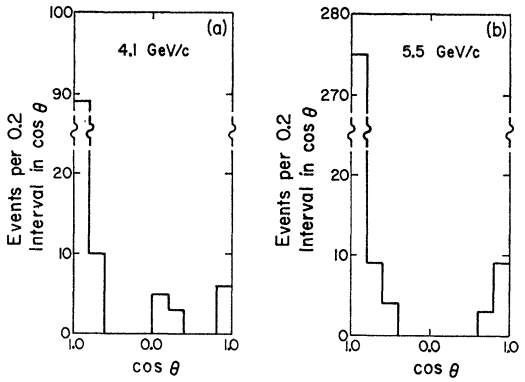

FIG. 1. Center-of-mass production angular distributions for $K^-p \to \Sigma^+\pi^-$. (a) 4.07 GeV/c, (b) 5.47 GeV/c. θ is the angle between the incoming K^- and the outgoing π^- in the center-of-mass frame. Note the broken scale in the forwardmost bin.

examined χ^2 distributions and "pull distributions"[12] for reactions (1) and (2) as well as for other reactions analyzed in an identical fashion; we find excellent agreement to the expected distribution in all cases.

Approximately 3% of all events from the scan list appear to be genuine candidates for Σ hypotheses, but cannot be handled for a variety of reasons. Some of these events, referred to as "geometry failures," have secondary interactions on outgoing tracks near the production vertex; others have a track which travels nearly in the direction of the chamber magnetic field; and others are obscured by electron whorls or other tracks in the chamber. We assume that the same fraction, 3%, have been lost from reactions (1) and (2).

We have applied the additional acceptance criterion that the χ^2 probability be greater than 0.02. Taken together, the χ^2 probability cut, the random scanning losses (4%), and the geometry failures (3%) imply a multiplicative factor of 1.09 to be applied to the number of identified events from reactions (1) and (2). Note that this correction is to be applied to all events in addition to the weight factor due to Σ detection.

III. EXPERIMENTAL RESULTS

The cross sections, corrected for Σ detection efficiency, for these reactions at 4.07 and 5.47 GeV/c are given in Table I. The center-of-mass angular distributions for reaction (1), corrected for Σ detection efficiency, are shown in Fig. 1. These distributions are dominated by the peripheral peak that is characteristic of two-body and quasi-two-body reactions above 1 GeV/c that proceed via meson exchange.[4,5] The forward peak contains

[12] If we denote the ith track variable by x_i and its error by σ_i, then the "pull" for the ith variable is defined by $(\text{pull})_i = (x_i^m - x_i^f)/[(\sigma_i^m)^2 - (\sigma_i^f)^2]^{1/2}$, where the superscript f refers to the fitted value and the superscript m refers to the measured value. If the estimates of error are correct, then the pull for all track variables should be normally distributed with a mean of zero and a standard deviation of unity. For a detailed discussion, see J. P. Berge, F. T. Solmitz, and H. D. Taft, Rev. Sci. Instr. 32, 538 (1961).

TABLE II. Differential cross section for $K^-p \to \Sigma^+\pi^-$ at 4.07 Gev/c.

c.m. cosine $\hat{p}_K \cdot \hat{p}_\pi$	$-t$ (GeV/c)^2	Observed events	Corrected events	$d\sigma/d\Omega$ (μb/sr)	$d\sigma/dt$ [μb/(GeV/c)^2]
1.000 to 0.975	−0.015 to 0.065	18	42±14	266±89	503±170
0.975 to 0.950	0.065 to 0.145	14	24± 9	146±55	278±105
0.950 to 0.925	0.145 to 0.225	6	8± 5	49±28	96± 56
0.925 to 0.875	0.225 to 0.384	7	10± 6	32±17	60± 32
0.875 to 0.800	0.384 to 0.624	4	7± 5	14±10	30± 21
0.800 to 0.650	0.624 to 1.103	6	14± 8	14± 8	30± 17

about 85% of the events at 4.07 GeV/c and about 95% of the events at 5.47 GeV/c. The cross section for producing "forward" events, σ_{forward}, is then 91±25 μb at 4.07 GeV/c and 80±14 μb at 5.47 GeV/c.

The details of the differential cross section for the peripheral region of reaction (1) are presented in Tables II and III and plotted in Fig. 2. The quoted errors are arbitrarily taken to be 1.4 times the statistical errors based on the number of observed events in each bin. We have multiplied the statistical errors by this factor in an attempt to include possible inaccuracies in our Σ weighting procedure. The importance of the Σ-detection problem is clearly seen by comparing the raw data with the corrected data in Tables II and III. The correction for Σ loss increases as $|t|$ decreases. For $|t|$ near zero, the average correction is about 2.0, whereas for $|t|$ near 0.3 (GeV/c)^2, the average correction is about 1.5. This t dependence arises because events with small $|t|$ have small Σ laboratory momenta. Such events tend to have short Σ tracks and hence large corrections for detection efficiency, as explained in the Appendix.

For reaction (1) we have made a parametrization of the data in the forward peak of the form

$$\frac{d\sigma}{dt}=\left(\frac{d\sigma}{dt}\right)_0 \exp[A(t-t_0)].$$

The kinematic maximum for t is denoted by t_0. Our best estimates for A and $(d\sigma/dt)_0$, presented in Table IV, are based on fits for $|t| \lesssim 0.5$ (GeV/c)^2. The solid curves superimposed on Fig. 2 correspond to these values. The parameter A is somewhat dependent on the t range chosen, since the data are not purely exponential. The differential cross section at t_0, $(d\sigma/dt)_0$, is found from the relation

$$\sigma_{\text{forward}}=\int \left(\frac{d\sigma}{dt}\right)_0 \exp[A(t-t_0)]dt=\left(\frac{d\sigma}{dt}\right)_0/A\,,$$

where σ_{forward} is estimated from the fraction of events found in the forward peak. The errors which we assign to A and $(d\sigma/dt)_0$ reflect both the fitted error and the instability of the parameters with respect to the t range chosen.

In reactions (1) and (2), events in the backward region ($\hat{K}\cdot\hat{\pi}\approx -1$) are of interest, since they may be produced by baryon exchange. With our present statistics, however, we can only make crude estimates for the backward cross sections. For this purpose, we list in Table V the center-of-mass production angle for backward-hemisphere events from reaction (1) and for all events from reaction (2). In Table VI we estimate the differential cross section averaged over the center-of-mass cosine interval from −0.9 to −1.0. In making these estimates, each observed event has been given a detection weight of 1.5 to 2.0 (see Appendix). An additional factor of 2 has been applied to the events of reaction (1), since in the backward hemisphere only the $\Sigma^+ \to \pi^+ n$ decay mode can be seen.

IV. COMPARISON WITH OTHER EXPERIMENTS

Recently, Morrison compiled cross sections for many two-body and quasi-two-body processes.[13] In Fig. 3, we show a plot of cross sections for reactions (1) and (2), taken from Morrison's paper, on which we have placed our measured cross sections. Our data continue the trends established by experiments at lower momenta.

[13] D. R. O. Morrison, Phys. Letters **22**, 528 (1966).

TABLE III. Differential cross section for $K^-p \to \Sigma^+\pi^-$ at 5.47 GeV/c.

c.m. cosine $\hat{p}_K \cdot \hat{p}_\pi$	$-t$ (GeV/c)^2	Observed events	Corrected events	$d\sigma/d\Omega$ (μb/sr)	$d\sigma/dt$ [μb/(GeV/c)^2]
1.000 to 0.975	−0.011 to 0.101	70	140±24	242±42	338±58
0.975 to 0.950	0.101 to 0.213	41	77±17	133±29	186±41
0.950 to 0.925	0.213 to 0.325	21	32±10	55±17	78±24
0.925 to 0.900	0.325 to 0.437	3	5± 4	9± 7	12±10
0.900 to 0.875	0.437 to 0.549	6	10± 6	18±10	27±16
0.875 to 0.850	0.549 to 0.660	4	7± 5	14±10	19±14
0.850 to 0.800	0.660 to 0.884	6	10± 6	9± 5	12± 7
0.800 to 0.700	0.884 to 1.332	2	3± 3	1± 1	2± 2

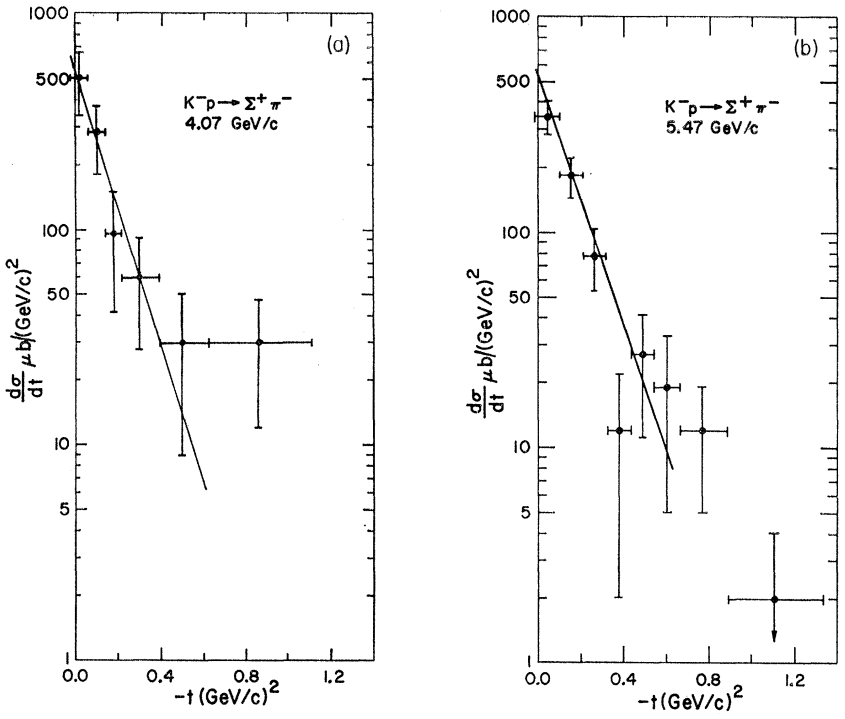

FIG. 2. Differential cross section in the peripheral region for $K^-p \to \Sigma^+\pi^-$: (a) 4.07 GeV/c, (b) 5.47 GeV/c. The solid curve is the result of a fit of the form $d\sigma/dt = (d\sigma/dt)_0 \exp[A(t-t_0)]$.

Morrison points out that many two-body and quasi-two-body reactions are well represented by the expression

$$\sigma = \text{const} \times (p_{\text{lab}})^{-n},$$

where p_{lab} is the incident laboratory momentum, and n is constant for any given process. Morrison concludes that for elastic reactions, $n \approx 0$; for nonstrange-meson–exchange reactions, $n \approx 1.5$; for strange-meson–exchange reactions, $n \approx 2.0$; and for baryon-exchange reactions, $n \approx 4$.

Using the above expression, we have made a least-squares fit to the cross-section values above 1.47 GeV/c for reaction (1). On the basis of six measurements, we find $n = 1.8 \pm 0.4$, This value is consistent with the exchange of strange mesons according to Morrison's prescription. Further evidence for meson exchange is seen in the center-of-mass production angular distribution, where the peripheral peak becomes more dominant as the incident K^- momentum increases. This feature is summarized by Table VII, in which we estimate the percentage of observed events found in the forward peak[14] as a function of incident K^- momentum.

TABLE IV. Values of A and $(d\sigma/dt)_0$.

K^- momentum (GeV/c)	A (GeV/c)$^{-2}$	$(d\sigma/dt)_0$ [mb/(GeV/c)^2]
4.07	7.3±1.3	0.66±0.21
5.47	6.7±0.7	0.54±0.12

[14] By "forward peak" we mean all events for which $\hat{K}\cdot\hat{\pi}$ is greater than zero in the center-of-mass system after subtracting any isotropic component in this distribution.

There is evidence for baryon exchange for both reaction (1) and (2) at lower momenta. For reaction (1), there is a noticeable backward peak at 3.5 GeV/c,[3] corresponding to a backward differential cross section of approximately 10 μb/sr; for reaction (2), there are clear backward peaks at 2.24,[1] 3.0,[2] and 3.5 GeV/c,[3] corresponding to backward differential cross sections of approximately 20, 15, and 5 μb/sr, respectively. Our estimates for these cross sections at 4.07 and 5.47 GeV/c (see Table VI) are consistent with the lower-energy results and with a rapidly decreasing baryon-exchange production as expected on the basis of Morrison's observations. Unfortunately, our data are too poor to make a good test of the $SU(3)$ prediction of equality between

TABLE V. List of center-of-mass cosines for all $\Sigma^-\pi^+$ events and for backward-hemisphere $\Sigma^+\pi^-$ events.

Reaction	Event	4.07 GeV/c c.m. prod. cosine $(\hat{K}\cdot\hat{\pi})$	Event	5.47 GeV/c c.m. prod. cosine $(\hat{K}\cdot\hat{\pi})$
$K^-p \to \Sigma^+\pi^-$ (backward-hemisphere events)	1	−0.095	1	−0.678
	2	−0.139	2	−0.926
	3	−0.337	3	−0.974
	4	−0.951		
	5	−0.973		
$K^-p \to \Sigma^-\pi^+$ (all events)	1	0.963	1	0.776
	2	0.538	2	0.246
	3	0.160	3	−0.718
	4	−0.577	4	−0.950
	5	−0.598	5	−0.951
	6	−0.974	6	−0.973

TABLE VI. Backward differential cross sections for $K^-p \to \Sigma^\pm\pi^\mp$ at 4.07 and 5.47 GeV/c.

Reaction	Momentum (GeV/c)	$\frac{d\sigma}{d\Omega}$ (μb/sr), averaged over $-0.9 \geq \hat{K}\cdot\hat{\pi} \geq -1.0$
$K^-p \to \Sigma^+\pi^-$	4.07	9±7
	5.47	3±2
$K^-p \to \Sigma^-\pi^+$	4.07	3±3
	5.47	2±2

the $K^-p \to \Sigma^+\pi^-$ and $\pi^-p \to \pi^-p$ backward cross sections, although our data are not inconsistent with such an equality.[15]

V. APPLICATION OF THE REGGE-POLE MODEL TO $K^-p \to \Sigma^+\pi^-$

In the past few years, the Regge model has had impressive successes at high energy ($p_{\text{lab}} \gtrsim 3$ GeV/c) in fitting the energy and momentum transfer dependence of elastic and charge-exchange reactions initiated by πN, KN, and $\bar{K}N$. Generally, the approach has been phenomenological in the sense that the Regge model has been used as a framework for parametrization of existing experimental data. The idea has been to find a self-consistent set of parameters that can account for

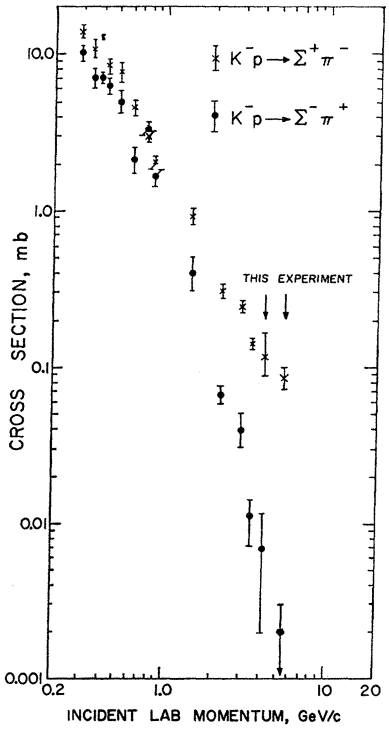

FIG. 3. Cross sections for $K^-p \to \Sigma^\pm\pi^\mp$ versus incident laboratory momentum. This figure is taken from Morrison (Ref. 13). The points at 4.07 and 5.47 GeV/c (this experiment) have been added for both reactions.

[15] V. Barger, Rev. Mod. Phys. 40, 129 (1968).

TABLE VII. σ_{forward} for $K^-p \to \Sigma^+\pi^-$ above 2.0 GeV/c.

K^- momentum (GeV/c)	Reference	$\sigma(K^-p \to \Sigma^+\pi^-)$ (μb)	% forward peak	Estimated σ_{forward} (μb)
2.24	2	295±29	60±10	177±33
3.0	3	236±17	70±10	165±28
3.5	5	140±10	80±10	112±17
4.07	this expt.	107±29	85± 5	91±25
5.47	this expt.	84±14	95± 2	80±14

wide ranges of energy and momentum transfer for many different reactions simultaneously. Interpretation of the parameters by means of symmetry or dynamical arguments is considered a separate task.

Because the phenomenological approach is linked intimately to experimental data, up to the present time, little Regge-model work has been done on strangeness-exchange reactions, owing to the paucity of experimental data. The earliest attempt to perform a Regge analysis on the $K^-p \to \Sigma^+\pi^-$ reaction was made by Iwao[6] in terms of a single $K^*(890)$ exchange. More recently, Arnold[7] has undertaken a more ambitious project to relate the π^-p charge-exchange reaction to several strange-meson–exchange processes, including $K^-p \to \Sigma^+\pi^-$. In his analysis, Arnold has used both the $K^*(890)$ and $K^*(1420)$ trajectories (hereafter referred to as the q and Q trajectories). In order to connect the strange-meson–exchange reactions to one another and to the π^-p charge-exchange reaction, Arnold employs $SU(3)$ symmetry arguments to find relations between the various residue factors. In addition, he assumes that the q and Q trajectories are degenerate functions of t (exchange degeneracy) and that they are parallel to the ρ trajectory. The predictions that Arnold makes are for $t=0$, where the helicity-flip contributions may be ignored. Although there is fair agreement between Arnold's predictions and some of the available experimental data, our values for $d\sigma/dt$ at $t=0$ are in clear disagreement. We find values of 660±210 and 540±120 mb/(GeV/c)^2 at 4.07 and 5.47 GeV/c, respectively, to be compared with Arnold's predictions of ~250 and ~125 mb/(GeV/c)^2.

The most recent Regge analysis for q and Q trajectory exchange processes has been done by Sarma and Reeder[8] in connection with the following reactions:

$$\pi^-p \to K^0\Lambda, \quad \text{(a)}$$

$$K^-p \to \pi^0\Lambda, \quad \text{(b)}$$

$$\pi^+p \to K^+\Sigma^+, \quad \text{(c)}$$

$$\pi^-p \to K^0\Sigma^0, \quad \text{(d)}$$

$$K^-p \to \pi^-\Sigma^+. \quad \text{(e)}$$

In their analysis, our data at 4.07 and 5.47 GeV/c have been used as part of the input data for reaction (e). In order to make a detailed comparison of our data for

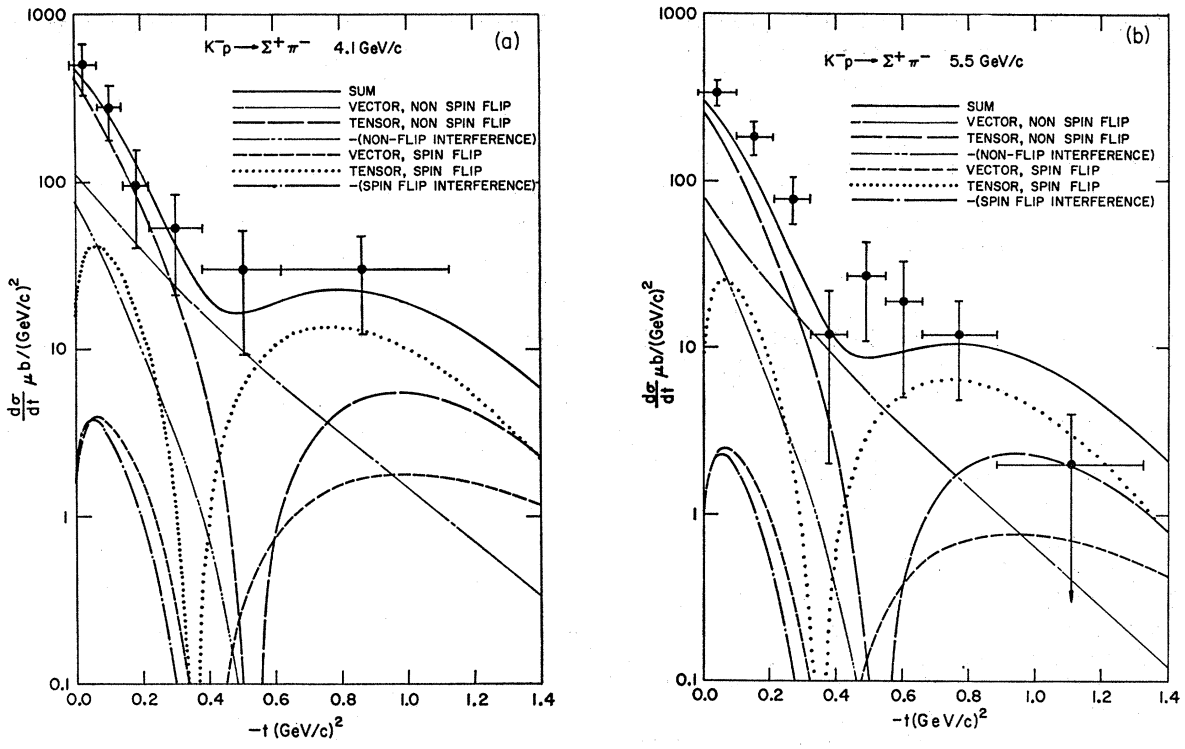

FIG. 4. Regge prediction of Sarma and Reeder for the reaction $K^-p \to \Sigma^+\pi^-$. (a) 4.07 GeV/c, (b) 5.47 GeV/c. The experimental points are from this experiment. The solid curve is the prediction of Sarma and Reeder and is the summation of the contributions from the various sources indicated.

reaction (e) with the results of Sarma and Reeder, we briefly summarize their formalism below.

The differential cross section is given by

$$d\sigma/dt \propto |F_{++}|^2 + \phi|F_{+-}|^2,$$

where F_{++} is the helicity-nonflip amplitude, F_{+-} is the helicity-flip amplitude, and ϕ is a kinematical factor proportional to $\sin^2\theta$, where θ is the c.m. scattering angle. Since both q and Q trajectories are assumed to participate, F_{++} and F_{+-} are each the sum of two terms. On the basis of isospin symmetry, charge-conjugation invariance, and parity invariance, the amplitudes for reactions (c), (d), and (e) may be written as

$$\begin{aligned} F_{+\pm} &= G_{+\pm}(q) + G_{+\pm}(Q) && \text{for reaction (c)}, \\ F_{+\pm} &= \tfrac{1}{2}\sqrt{2}G_{+\pm}(q) + \tfrac{1}{2}\sqrt{2}G_{+\pm}(Q) && \text{for reaction (d)}, \\ F_{+\pm} &= -G_{+\pm}(q) + G_{+\pm}(Q) && \text{for reaction (e)}. \end{aligned}$$

The Regge amplitudes adopted by Sarma and Reeder are of the form

$$G_{+\pm}(q) = C_\pm(q)\gamma_{+\pm}(q)[i + \tan(\tfrac{1}{2}\pi\alpha_q)] \times (\alpha_q+1)^2 \begin{Bmatrix} 1 \\ \alpha_q \end{Bmatrix} R_\pm(q),$$

$$G_{+\pm}(Q) = C_\pm(Q)\gamma_{+\pm}(Q)[i - \cot(\tfrac{1}{2}\pi\alpha_Q)]\alpha_Q \times (\alpha_Q+1) \begin{Bmatrix} (1+t/t_Q) \\ \alpha_Q \end{Bmatrix} R_\pm(Q),$$

where $C_\pm$ are $SU(3)$ coefficients, $\gamma_{+\pm}$ are the residue factors, α_q and α_Q are the trajectory functions, and t_Q is a "crossover" factor which forces $G_{++}(Q)$ to zero at $-t=t_Q$. The factor $R_\pm$ is given by

$$R_\pm(e) = \left[\frac{s - \tfrac{1}{2}(m_1^2+m_2^2+m_3^2+m_4^2-t)}{(m_1+m_2)E_\pm(e)}\right]^{(\alpha_e-\frac{1}{2})\pm\frac{1}{2}},$$

where $E_\pm(e)$ is an energy-scale factor for e exchange, m_1 and m_2 are the baryon masses, and m_3 and m_4 are the meson masses.

Note that in the two-pole model there are six terms which contribute to $d\sigma/dt$:

(1) q helicity nonflip,
(2) Q helicity nonflip,
(3) nonflip interference between q and Q,
(4) q helicity flip,
(5) Q helicity flip,
(6) helicity-flip interference between q and Q.

Using the fitted parameters of Sarma and Reeder, we have evaluated these six terms for reaction (e) at 4.07 and 5.47 GeV/c. The results are shown in Fig. 4, along with our experimental data points. The summation of the six terms fits our data rather well out to $-t \sim 0.8$ (GeV/c)^2, except that at 5.47 GeV/c the prediction seems to be about 20% low. The dip which appears for $-t \sim 0.5$ is perhaps suggested by the data, but not required.

There are two features that we wish to point out in Fig. 4. First, the Q-trajectory terms dominate the reaction everywhere except in the vicinity of the dip. To the left of the dip, the Q nonflip amplitude dominates, while to the right of the dip, the Q helicity-flip amplitude dominates. The second feature that we wish to mention is that the zero in the Q-nonflip amplitude for $|t|=0.56$ (GeV/c)^2 is due to the presence of the "crossover" factor $(1+t/t_Q)$ in the Q-nonflip amplitude. If this factor is removed and all other parameters are held fixed, the Q-nonflip amplitude dominates the reaction out to a $|t|$ value of about 0.6 (GeV/c)^2 and therefore fills in much of the dip region. Were the $(1+t/t_Q)$ factor omitted in the fitting procedure, the values of the parameters for the best fit, at least for our reaction at our energies, might be quite different. Even without the $(1+t/t_Q)$ factor, a dip could still result from the vanishing of the helicity-flip q and Q amplitudes corresponding to zeros in their respective trajectory functions in the vicinity of $-t=0.4$ (GeV/c)^2.

The statistical and systematic uncertainties inherent in the present experiment unfortunately limit the number of definitive conclusions that can be made about the details of the Sarma-Reeder model. The validity of the $(1+t/t_Q)$ term, for example, cannot be precisely tested by the present experiment. However, whether or not all of the details of the Sarma-Reeder model are correct, we can conclude that the model does provide a reasonable fit to our data and that the Regge model can indeed be fruitfully employed to explain the s and t dependence of a number of hypercharge-exchange reactions.

ACKNOWLEDGMENTS

We are grateful for the assistance given to us by the ZGS and bubble-chamber staffs at the Argonne National Laboratory. We also wish to acknowledge the capable work of many individuals, too numerous to mention, on the scanning and measuring crews, the supervisory staff, the engineering staff, and the programming staff at the University of Illinois.

APPENDIX: Σ DETECTION AND WEIGHTING

1. Introduction

In this Appendix, we discuss the problems associated with the detection of charged Σ tracks. Although this paper reports only on two-body final states, we assume that problems of Σ detection do not depend crucially on the particular final states. Therefore we have investigated a sample of about 1800 events, taken from the 5.47-GeV/c data, in which a charged Σ is produced in a two-, three-, four-, or five-body final state. Obvious nonhyperon decays, Ξ^- events, and events with a χ^2 probability less than 0.1 have been removed from the sample.

Because the detection of events with a charged Σ depends upon the visual observation of the hyperon decay, there are two outstanding detection problems, namely, (1) very short Σ tracks and (2) very small laboratory decay angles between the Σ and its charged decay product. The first problem is associated primarily with events for which the Σ laboratory momentum is low, whereas the second occurs primarily for events with high Σ momentum. Since these two effects occur in nearly disjoint momentum regions, we have examined the two detection problems separately, and have then combined them so that the final weighting formula is the product of a factor which depends on Σ length and a factor which depends on the decay angle. The corrections for Σ length are discussed in Sec. 2 and those for small decay angle are discussed in Sec. 3. In Sec. 4, we summarize the procedure for the combined weights.

For the $K^-p\rightarrow\Sigma^+\pi^-$ reaction, reported in this paper, the peripherally produced Σ^+ particles tend to have low laboratory momenta (about 80% of these events have Σ momenta between the lower kinematic limit of 0.25 and 0.8 GeV/c). Consequently the main correction for these events is for short Σ loss (Sec. 2).

2. Correction for Σ-Length Detection

Figure 5 shows the length distribution for all Σ^+ and Σ^- events in the detection-study sample for which the hyperon momentum is in the interval from 0.3 to 1.1 GeV/c. The solid curve is the expected distribution, obtained in the following way. First, all Σ^+ (or Σ^-) events from a given small momentum interval (e.g., from 0.5 to 0.7 GeV/c) are plotted. Then, the expected length distribution is computed corresponding to the average momentum of the interval (0.6 GeV/c, in our example) and normalized to the number of events having Σ lengths between 1.0 and 10.0 cm. When the Σ^+ and Σ^- curves for all momentum intervals are summed, the solid curve of Fig. 5 is obtained.

Figure 5 shows clearly that there is a detection bias in our data against Σ tracks shorter than about 1.0 cm.

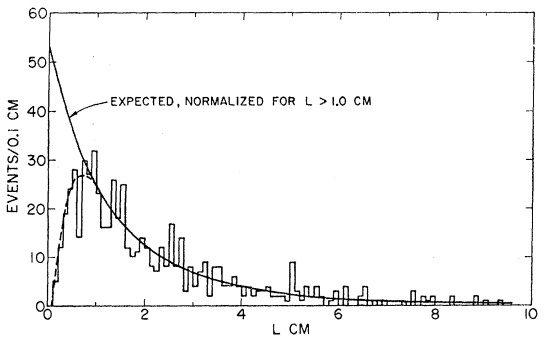

FIG. 5. Observed and expected Σ-length distributions for events with Σ momenta between 0.3 and 1.1 GeV/c. The solid curve is the expected distribution normalized to $L>1.0$ cm (see text). The dashed curve is our hand-drawn representation of the observed length spectrum. The ratio of the heights of the two curves determines an empirical detection efficiency as a function of Σ length.

The dashed curve is our hand-drawn smoothed representation of the length spectrum. The correction factor (i.e., the reciprocal of the detection efficiency) as a function of Σ track length is just given by the ratio of the height of the solid curve to that of the dashed curve. We find that this ratio can be parametrized empirically by the following expression:

$$W_1(L)=1+C\exp(-L/L_0), \qquad \text{(A1)}$$

where L is the length of the Σ track, $C=12.0$, and $L_0=0.16$ cm. Since this expression becomes large for $L \lesssim 0.4$ cm, we have chosen the minimum Σ-length cutoff to be 0.5 cm.

There are two other Σ-length-detection considerations of minor importance. First, a small loss of events with long Σ tracks is expected because of the finite chamber size. Second, in order to eliminate obvious nonhyperon events, we have rejected all events in which the Σ lives more than 5 mean lifetimes.

It is necessary to correct for events lost beyond our cutoffs. The weight favor $W_2(p)$ corresponding to the imposed cutoffs is simply the reciprocal of the probability that the event would have survived the acceptance criteria

$$W_2(p)=\{\exp[-L_{\min}/\lambda(p)]-\exp[-Q(p)]\}^{-1}, \qquad \text{(A2)}$$

where $L_{\min}=0.5$ cm, p is the Σ momentum, $\lambda(p)=(pc\tau)/m=$ mean Σ length, m is the Σ mass, τ is the Σ lifetime, $Q(p)$ is the minimum of either $[s/\lambda(p)]$ or N_τ, s is the distance in the direction of the Σ track to the edge of the chamber volume, and N_τ is the maximum number of allowed Σ lifetimes. As stated above, $L_{\min}$ was chosen to be 0.5 cm; the distance s was computed for each event; N_τ was chosen to be 5 lifetimes. The second exponential in (A2) contributes only about a 1% correction to the Σ^+ events and only about a 4% correction to the Σ^- events.

3. Correction for Small Decay Angles

Turning now to the problem of detecting small laboratory decay angles between the Σ and its charged decay product, we again compare observed distributions with expected distributions in order to determine an empirical detection efficiency as a function of decay angle. For this comparison we have chosen, from the 5.47-GeV/c data, events having a Σ momentum greater than 1.3 GeV/c and having one of the two charged pionic decays ($\Sigma^\pm \to \pi^\pm n$). Events with the proton decay ($\Sigma^+ \to p\pi^0$) have been excluded because, as discussed later, these decays have a much more severe decay-angle loss than the other modes.

Figure 6 shows the experimental distribution for θ, defined as the laboratory decay angle between the Σ and its charged decay product, along with the expected θ distribution (solid curve) which has been normalized for θ greater than 15°. The expected curve has been generated in the following way. For each of several narrow Σ laboratory momentum intervals, we first generate (via Monte Carlo) a uniform decay-angle population in the Σ rest frame. Then this distribution is transformed to the laboratory frame and is normalized to the observed spectrum for θ greater than 15°. When the curves from the several laboratory momentum intervals are summed, the result is the solid curve in Fig. 6. The dashed curve is our hand-drawn representation of the data. It is clear that there is a loss of events which have decay angles less than about 15°. The empirical correction for decay-angle loss as a function of θ is just given by the ratio of the height of the solid curve to that of the dashed curve. We find that this ratio can be parametrized by the following expression:

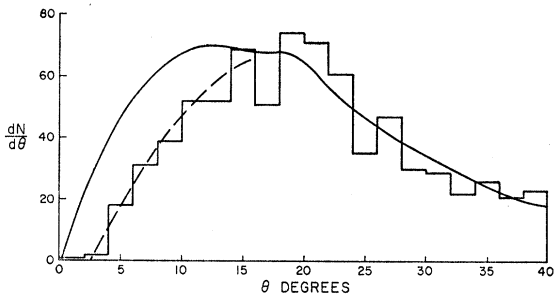

FIG. 6. Observed and expected laboratory-decay-angle distributions for events with Σ momenta greater than 1.3 GeV/c. The solid curve is the expected distribution, generated by a Monte Carlo technique and normalized to the number of events having decay angles greater than 15° (see text). The dashed curve is our hand-drawn representation of the data. The ratio of the heights of the two curves determines an empirical detection efficiency as a function of decay angle.

$$W_3(\theta)=\exp\left[\left(\frac{\theta_2-\theta}{\theta_1}\right)^2\right], \quad \text{for } \theta<\theta_2$$
$$=1, \quad \text{for } \theta>\theta_2 \qquad \text{(A3)}$$

where θ is the laboratory decay angle between the Σ and its charged decay product, $\theta_1=14°$, and $\theta_2=18°$. Since $W_3(\theta)$ becomes very large for θ values less than about 5°, we have chosen our minimum θ, cutoff $\theta_{\min}$, to be 7°.

To compensate for the $\theta_{\min}$ cutoff, each accepted event must be weighted by the reciprocal of the probability that θ is greater than $\theta_{\min}$. Assuming that the decay angular distribution in the rest frame of the Σ is isotropic, we then weight each accepted event by the expression

$$W_4(p)=2/[\cos\alpha(p)-\cos\beta(p)], \qquad \text{(A4)}$$

where p is the laboratory Σ momentum, and $\alpha(p)$, $\beta(p)$ are the decay angles in the Σ rest frame corresponding to a laboratory decay angle $\theta_{\min}$ and a laboratory Σ momentum p.

In the case of the charged pionic decays, the decay-angle losses are not severe for any Σ momentum region

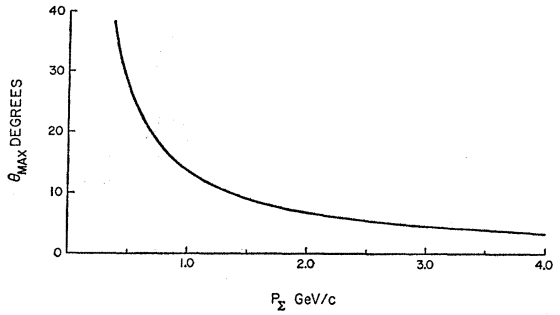

FIG. 7. Maximum laboratory decay angle for the decay $\Sigma^+ \rightarrow p\pi^0$. Detection loss becomes noticeable at a Σ momentum of about 0.8 GeV/c. Above 2.0 GeV/c the loss is severe.

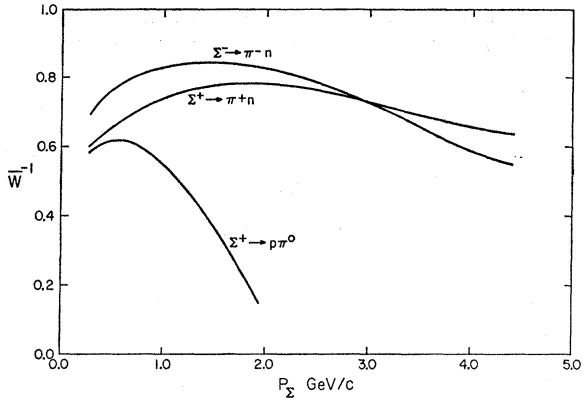

FIG. 8. Reciprocal of the average weight as a function of Σ momentum. Cutoffs for minimum laboratory decay angle and minimum Σ length have been imposed. The curves are obtained by dividing the weighted momentum spectra by the unweighted spectra. For K^-p interactions at 4.07 and 5.47 GeV/c, the lower kinematic limit for Σ momentum is about 0.25 GeV/c.

up to 5.0 GeV/c. On the other hand, the decay-angle loss is severe for the proton-decay mode for momenta above about 1.5 GeV/c, as is illustrated in Fig. 7. This plot shows the maximum kinematically allowed laboratory decay angle, for the proton-decay mode, as a function of Σ laboratory momentum. Nevertheless, for Σ momenta below 1.5 GeV/c, we find that the procedure developed above is adequate for the weighting of the $\Sigma^+ \rightarrow p\pi^0$ decays.

4. Combined Weights

Whenever an individual event survives all of the aforementioned cutoffs, that event is given a weight $W(L,\theta,p)$ which is the product of the preceding weight factors:

$$W(L,\theta,p) = W_1(L)W_2(p)W_3(\theta)W_4(p). \quad \text{(A5)}$$

Although this weighting prescription is applied to individual events, the average weight for each decay mode as a function of Σ momentum may be found by dividing the Σ momentum spectrum of the weighted events by that of the unweighted events. In Fig. 8, we show the smoothed curves for the reciprocal of the average weight obtained by such divisions. The difference in weighting between the two pionic modes is caused mainly by the difference in the lifetimes of the Σ^+ and Σ^-. Because of the kinematic restriction on the decay angle for the proton-decay mode (discussed above), it appears unsafe to use weighted events from this decay mode when the Σ momentum is greater than about 1.5 GeV/c.

This weighting prescription, although developed from the observed data at 5.47 GeV/c, is found to be satisfactory for the 4.07-GeV/c data as well.